JOURNAL OF PROPULSION AND POWER
Vol. 11, No. 6, November–December 1995

Simulation of Laminar–Turbulent Transition with an Explicit Navier–Stokes Flow Solver

Lyle D. Dailey* and Ian K. Jennions†
General Electric Aircraft Engines, Cincinnati, Ohio 45215
and
Paul D. Orkwis‡
University of Cincinnati, Cincinnati, Ohio 45221

A low Reynolds number (LRN) k-ε turbulence model has been implemented in a three-dimensional Navier–Stokes flow solver such that laminar–turbulent boundary-layer transition can be simulated. This was done in an attempt to improve the loss prediction of the code that had previously used wall functions and assumed fully turbulent flow. These assumptions can lead to an overprediction of the loss for turbomachinery blade rows containing significant regions of transitional flow. This article details the problems associated with implementing a LRN k-ε model in an explicit Navier–Stokes flow solver and presents results from testing the model on zero pressure gradient flat plate flow at various freestream turbulence intensities and length scales. The results are compared to experimental data and a two-dimensional boundary-layer code that utilizes the same turbulence model. The addition of the LRN turbulence model improved the loss prediction capability of the Navier–Stokes (NS) code, and the chosen length scale had a large effect on the predicted loss. The sensitivity to the near-wall grid, convergence and stability problems, and excessive run times make the LRN k-ε model in an explicit NS code impractical for design applications at this time.

Nomenclature

C_d = drag coefficient
C_f = skin friction coefficient
C_μ, C_1, C_2 = k-ε equation constants
DX = axial grid spacing for uniform part of grid for Navier–Stokes code
DXR = ratio of streamwise gid spacing to boundary-layer thickness for boundary-layer code
f_μ, f_1, f_2 = damping functions for k-ε model
k = turbulent kinetic energy
L = inlet turbulence length scale
NBL = number of grid cells across boundary layer for boundary-layer code
NX = total number of grid cells along plate
NY = total number of grid cells normal to plate
$N30$ = number of grid cells below $y^+ = 30$
$N4K$ = number of grid cells before $Re_x = 10^4$
P = turbulence production
$REXMIN$ = Re_x for initial profiles for boundary-layer code
$REX1$ = Re_x of first grid cell near leading edge for Navier–Stokes code
Re_L = Reynolds number based on length of plate
Re_t = turbulence Reynolds number, $k^2/\nu\varepsilon$
Re_x = Reynolds number based on x
Re_y = Reynolds number based on distance from wall, $\sqrt{k}y/\nu$
Re_θ = momentum thickness Reynolds number
Rex, e = Re_x at end of transition
Rex, t = Re_x at start of transition
$TU0$ = inlet freestream turbulence intensity
u_i = Cartesian velocity components
V_{inlet} = inlet freestream velocity
x_i = Cartesian coordinates
y = normal distance from wall
y^+ = normalized distance to wall, $y\sqrt{\tau_w\rho}/\mu_l$
y_1^+ = y^+ for first grid cell near wall
ε = turbulent dissipation rate
μ_l = molecular viscosity
μ_t = turbulent viscosity
ν = kinematic viscosity
ρ = density
σ_k, σ_ε = k-ε equation constants
τ_w = wall shear stress

Received Nov. 29, 1993; presented as Paper 94-0189 at the AIAA 32nd Aerospace Sciences Meeting and Exhibit, Reno, NV, Jan. 10–13, 1994; revision received Jan. 24, 1995; accepted for publication Jan. 31, 1995. Copyright © 1994 by the American Institute of Aeronautics and Astronautics, Inc. All rights reserved.

*Engineer, Computational Turbomachinery Aerodynamics; currently Graduate Student at Iowa State University, Ames, Iowa. Student Member AIAA.

†Manager, Computational Turbomachinery Aerodynamics; currently Manager, CFD Technology at ABB Power Generation Ltd., Baden, Switzerland. Member AIAA.

‡Assistant Professor, Department of Aerospace Engineering and Engineering Mechanics. Member AIAA.

Introduction

ALTHOUGH current gas turbine engines are very efficient machines, there are still gains to be made through understanding and controlling the individual loss-producing mechanisms. The source of loss investigated in this article is that associated with the blade surface boundary layers. Many existing Navier–Stokes (NS) codes assume that the boundary-layer flow is turbulent from the leading edge. However, the Reynolds number is relatively small in low-pressure turbines, ranging from 4×10^5 to 8×10^5 (Ref. 1), which produces significant regions of laminar and transitional flow. High-pressure compressor blade rows can also have large regions of laminar and transitional flow.[2] In addition, transonic fans can have laminar flow before the shock and in the subsonic hub sections. Consequently, assuming the boundary layer to be turbulent from the leading edge can overpredict the loss as a result of neglecting the laminar portion of the boundary layer. If the effect of transition can be accounted for in these codes, turbomachinery blade designers can better tailor blade shapes to minimize loss over the entire engine operation range.

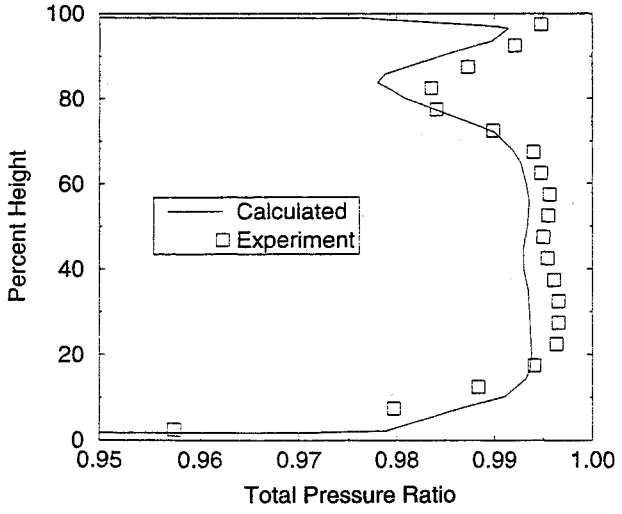

Fig. 1 Downstream total pressure profile for the E^3 low-pressure turbine first-stage vane using the HRN k-ε turbulence model with wall functions.

The explicit three-dimensional Navier–Stokes flow solver for turbomachinery blade rows used in this work was described in detail by Turner and Jennions.[3] The code does reasonably well at predicting the loss for blade rows dominated by shock losses, such as transonic fans[4] and some high-pressure turbines.[5] This is not the case, however, for blade rows dominated by profile loss, such as in low-pressure turbines. Figure 1, e.g., shows the predicted and experimentally measured total pressure profiles downstream of the GE/NASA Energy Efficient Engine (E^3) low-pressure turbine first-stage vane. Although the large loss region (total pressure deficit) from 70–95% span, associated with the end-wall boundary layer separating at the vane leading edge, was predicted quite well, the loss on the remaining part of the blade was overpredicted.

One plausible reason for the overprediction is that many low-pressure turbine vanes are known to contain significant regions of laminar and transitional flow, as discussed earlier. The loss is overpredicted since the turbulence model uses wall functions and assumes turbulent flow over the whole blade surface. Therefore, the addition of a transition model should improve loss prediction and is the subject of this article.

Transition Models

Two commonly used turbulence models are the Baldwin–Lomax algebraic model[6] and the two-equation k-ε model.[7] A practical approach for predicting transitional flow is to extend these models. For a design code, this is seen as more desirable than using Reynolds stress models, large eddy simulation, or direct numerical simulation, because these approaches are too computationally intensive.

In this article, the LRN form of the k-ε model, which has been relatively successful in predicting laminar–turbulent boundary-layer transition in boundary-layer codes,[8] is investigated as a practical extension of an existing NS code. Comparisons are also made to the Baldwin–Lomax model with a point transition approach.

The LRN k-ε model of Lam and Bremhorst,[9] as modified by Rodi and Scheuerer,[10] was selected for the current work. An extensive literature review of available low Reynolds number (LRN) k-ε models revealed that the Lam–Bremhorst model was one of the best models for predicting laminar–turbulent transition.[11] Other models for which the damping functions are dependent on y^+ have been found to be unacceptable for transitional flow calculations.[11,12] In addition, the Lam–Bremhorst model uses the total dissipation rate as opposed to the isotropic dissipation rate, eliminating some additional terms for the k-ε transport equations that are difficult to implement in a general three-dimensional code. The Lam–Bremhorst model was also chosen since a two-dimensional boundary-layer code existed that utilized the same LRN k-ε model and, hence, could be used for comparison purposes. One disadvantage of the Lam–Bremhorst model is the dependence on y, which is difficult to define for complex three-dimensional geometries.

Description of Codes

The two codes used throughout the current work, a three-dimensional NS code and a two-dimensional boundary-layer (BL) code, are described in this section. The Lam–Bremhorst LRN k-ε model was implemented in the three-dimensional Navier–Stokes flow solver for turbomachinery blade rows described in detail by Turner and Jennions.[3] This code solves the full three-dimensional, compressible, Reynolds-averaged Navier–Stokes (RANS) equations for a single blade row. The unsteady RANS equations are marched in time to steady state using a cell centered, finite volume, explicit Runge–Kutta scheme. Second- and fourth-order Jameson-type smoothing is employed with Martinelli[13] anisotropic eigenvalue scaling for highly stretched grids. Local time stepping, multigrid acceleration, and implicit residual averaging with constant coefficients are used to accelerate or stabilize convergence. The code can be run inviscid, laminar, or turbulent with either the Baldwin–Lomax algebraic turbulence model[6] or the high Reynolds number (HRN) k-ε turbulence model with wall functions.[7]

The two-dimensional BL code described by Zerkle and Lounsbury[14] was used throughout this work to guide the research and for comparison purposes. This code is a two-dimensional, compressible, steady-state boundary-layer code that uses the Lam–Bremhorst LRN k-ε turbulence model as modified by Rodi and Scheuerer.[10] The code utilizes the pressure correction scheme developed by Patankar and Spalding.[15]

Implementation of LRN Model

The transport equations for the Lam–Bremhorst LRN k-ε model as modified by Rodi and Scheuerer[10] are

$$\frac{\partial(\rho u_j k)}{\partial x_j} = \frac{\partial}{\partial x_j}\left[\left(\mu_l + \frac{\mu_t}{\sigma_k}\right)\frac{\partial k}{\partial x_j}\right] + P - \rho\varepsilon \tag{1}$$

$$\frac{\partial(\rho u_j \varepsilon)}{\partial x_j} = \frac{\partial}{\partial x_j}\left[\left(\mu_l + \frac{\mu_t}{\sigma_\varepsilon}\right)\frac{\partial \varepsilon}{\partial x_j}\right] - f_1 C_1 \frac{\varepsilon}{k} P + f_2 C_2 \rho \frac{\varepsilon^2}{k} \tag{2}$$

$$P = \mu_t\left(\frac{\partial u_i}{\partial x_j} + \frac{\partial u_j}{\partial x_i}\right)\frac{\partial u_i}{\partial x_j}, \qquad \mu_t = f_\mu C_\mu \rho \frac{k^2}{\varepsilon} \tag{3}$$

The constants are $C_\mu = 0.09$, $C_1 = 1.44$, $C_2 = 1.92$, $\sigma_k = 1.0$, $\sigma_\varepsilon = 1.3$. In the HRN k-ε model, the damping functions, f_μ, f_1, and f_2, are all unity. For the LRN k-ε model, the functions are given by

$$f_\mu = [1 - \exp(-0.0165Re_y)]^2[1 + (20.5/Re_t)] \tag{4}$$

$$f_1 = 1 + (0.05/f_\mu)^3, \qquad f_2 = 1 - \exp(-Re_t^2) \tag{5}$$

The boundary conditions for k and ε are given by $k_{\text{wall}} = 0$ and $\varepsilon_{\text{wall}} = \nu\partial^2 k/\partial y^2$. However, the simpler but approximate boundary condition suggested by Patel et al.,[16] given by $d\varepsilon_{\text{wall}}/$

$dy = 0$, was used for the current work. Inlet conditions for k and ε are given by

$$k_{\text{inlet}} = \tfrac{3}{2}(TU0 \cdot V_{\text{inlet}})^2, \qquad \varepsilon_{\text{inlet}} = k_{\text{inlet}}^{3/2}/L \tag{6}$$

The k-ε equations are solved decoupled from the flow equations. The flow equations are iterated with a frozen turbulent viscosity field, then the flow variables are frozen and the k-ε equations are iterated to update the viscosity field. The k-ε equations are solved implicitly using an alternating direction implicit (ADI) approach.[3]

Convergence Issues

An average-error parameter was used for the convergence criterion. The average error is defined as the rms of the change in the absolute velocity for all grid cells, normalized by the rms of the absolute velocity and the Courant–Friedrichs–Lewy (CFL) multiplier, and multiplied by the cubed root of the number of grid cells. The average error is expressed as a percentage. For design purposes, the code is typically run such that the average error decreases by one or two orders of magnitude. For this work, the code was run to an average error level of 0.001%, which typically required a three- to four-order of magnitude decrease in the average error. This level of convergence was adequate to ensure negligible changes in the skin friction coefficient, the major parameter of interest for this work.

Convergence problems were encountered throughout this work because of the explicit solver and highly stretched near-wall grids required to solve the LRN k-ε equations. A much lower than normal CFL multiplier (a factor that multiplies the theoretical CFL number for the Runge–Kutta scheme) was required to maintain stability, resulting in slow convergence. The anisotropic eigenvalue scaling of Martinelli[13] was also necessary for the highly stretched grid. Similar problems were also reported by Kunz and Lakshminarayana[17] who solved the flow and HRN k-ε equations with an explicit Runge–Kutta scheme.

Problems with starting the solution were also encountered, as the LRN model was found to require good initial flow and turbulence fields. Typically, the converged solution from a HRN k-ε model on a coarser grid was interpolated onto the fine grid to start the LRN calculations. These starting problems were related to the large k and ε profile gradients that must be resolved near the wall.

Flat Plate Geometry

The NS code and corresponding grid generation system were designed to model turbomachinery blade rows. Therefore, a flat plate grid was created by generating a grid for a zero thickness, camber, and stagger angle blade row. Viscous wall boundary conditions were utilized on one blade surface, yielding the flat plate surface, and the other blade surface utilized inviscid wall boundary conditions to model the free-stream boundary. The inviscid wall was placed far enough away from the viscous wall to ensure that no pressure gradient developed in the passage. The regions upstream of the leading edge and downstream of the trailing edge were not modeled to minimize run times. Uniform conditions for the velocity field and turbulence properties (k and ε) were specified at the inlet, where boundary conditions were enforced by using ghost cells.

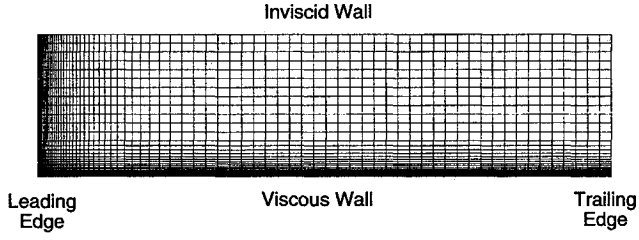

Fig. 2 Typical flat plate grid.

Only two-dimensional calculations were performed for this work, as the grid had a single grid cell in the spanwise direction. Hyperbolic tangent stretching was used both normal to the plate surface and in the streamwise direction. The grid was only stretched for the first 25% of the grid near the wall (normal to plate) and for the first 25% of the grid near the leading edge (along the plate). The remaining 75% of the grid had uniform spacing. A representative flat plate grid is shown in Fig. 2. Typically, the ratio of the maximum to minimum cell area was near 200,000, and cell ARs were as high as 2500.

Fully Laminar/Turbulent Results

The implementation of the LRN k-ε model in the NS code was tested by computing fully turbulent zero pressure gradient flat plate flows. Fully laminar calculations were also made for comparison purposes.

Run times for BL codes are relatively small, such that more than sufficient grid point density can be used to obtain grid independent results. However, the longer run times associated with a full NS code limit the grid that can be economically used. A grid study was thus conducted to determine how sensitive the NS code with LRN model might be to the near-wall grid for fully turbulent calculations.

The grid study involved running eight cases with various values of NY and y_1^+, where y_1^+ varied from 0.4 to 3.4, NY was either 64 or 80, and NX was 80. This led to values of $N30$ ranging from 4 to 21. The skin friction distributions were integrated over the flat plate to give the drag coefficient plotted vs $N30$ in Fig. 3. The predicted drag coefficient is seen to depend strongly on the number of grid cells in the near-wall region, and at least 10 grid cells were required to obtain less than 5% difference from White's[18] experimental correlation for fully turbulent, zero-pressure gradient, low-turbulence intensity flat plate flow. The reason for this strong dependence on $N30$ is evident in Fig. 4, which shows ε vs y^+ for four of the cases. A prediction from the BL code is also shown for comparison purposes. The BL code grid had y_1^+ values ranging from 0.004 at the leading edge to about 0.04 at the trailing edge, and $N30$ ranged from 95 to 58. Many grid cells are required below a y^+ of 30 to adequately resolve the large gradient and maximum in the ε profile.

Fully turbulent flat plate flow was also calculated with the other turbulence models available in the NS code. Figure 5 shows the skin friction as predicted with a fine grid (y_1^+ =

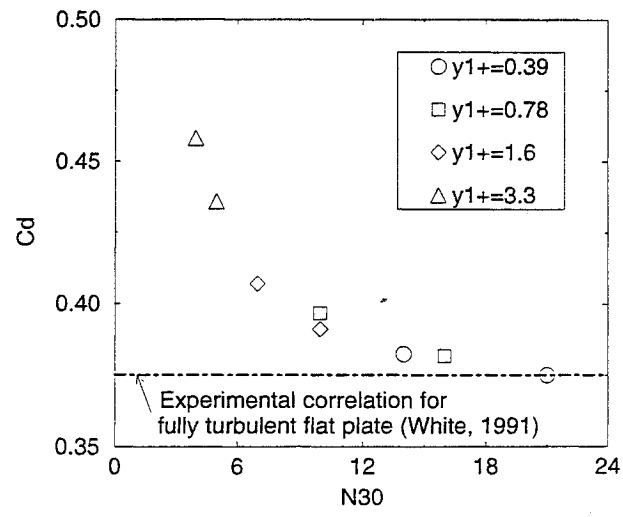

Fig. 3 Impact on loss prediction for fully turbulent flat plate with NS code ($Re_L = 2.9 \times 10^6$).

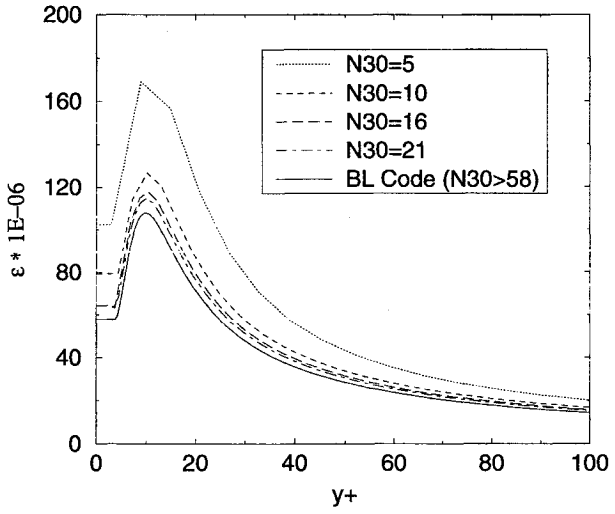

Fig. 4 Sensitivity to near-wall grid for LRN k-ε model with NS code ($Re_x = 2.4 \times 10^6$).

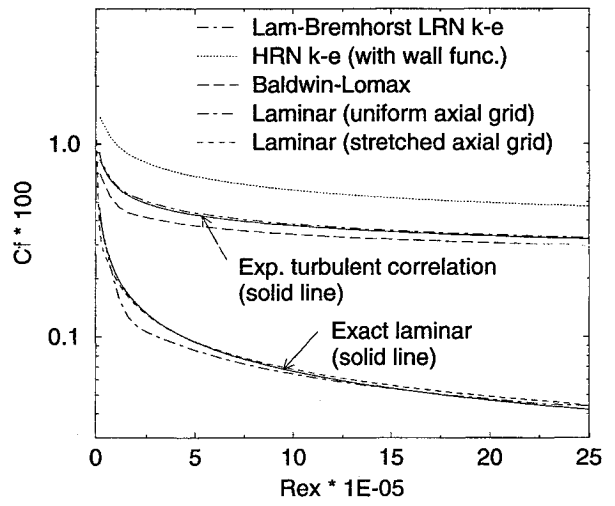

Fig. 5 Calculation of fully laminar or turbulent flat plate flow with NS code ($y\dagger = 0.39$, $N30 = 14$).

0.39 and $N30 = 14$) with the following models: HRN k-ε model with wall functions, LRN k-ε model, Baldwin–Lomax model with no wall functions, and laminar (no turbulence model). Note that as the use of the HRN k-ε model at such low y^+ values is not valid, the figure reveals large errors in the predictions for this model, as expected. The Baldwin–Lomax model and LRN k-ε model agree fairly well, with the LRN k-ε model showing better agreement with the experimental correlation.

Two laminar predictions are shown in Fig. 5, one with a uniformly spaced axial grid and one with a stretched axial grid. The laminar prediction with the uniform axial grid resulted in errors compared to the Blasius solution for the first 25% of the plate. Increasing the density of the axial grid near the leading edge by stretching the grid greatly improved the laminar prediction. This was an important consideration for later predictions of transitional flow.

Transitional Flow Predictions

BL Code Grid Sensitivity Study

The grid study already presented gave an indication of how sensitive the LRN model was for predicting fully turbulent flow. Another grid study was conducted to ascertain the grid sensitivity for transitional flow predictions. A study was first conducted with the BL code, for which many cases could be computed inexpensively, in hopes that the results would guide the grid study for the NS code.

The grid parameters that could be varied for the BL code are *NBL*, *DXR*, and *REXMIN*. For a given grid, the values of $y\dagger$ and *N*30 vary significantly from leading edge to trailing edge. For instance, for *NBL* = 94, $y\dagger$ ranges from 0.0036 at the leading edge to about 0.034 at the trailing edge, whereas *N*30 ranges from 94 to 58. At an axial location near the trailing edge ($Re_x = 4.8 \times 10^5$), *NBL* = 36, 60, and 94 results in $y\dagger$ taking the values of 0.04, 0.4, and 1.9 and *N*30 takes the values of 11, 25, and 58.

Figure 6 shows skin friction distributions for the BL code for *NBL* = 36, 60, and 94 for *TU*0 = 0.03 and 0.05. For grid-independent results, *NBL* must be at least 60 for *TU*0 = 0.05, and even larger for *TU*0 = 0.03. Figure 7 shows predictions for various streamwise step sizes (*DXR*). The results were more sensitive to this parameter, but it appears that grid independent results could be obtained if *DXR* was small enough.

The effect of varying *REXMIN* is shown in Fig. 8, which reveals that the transition location is not independent of *REXMIN* as *REXMIN* is decreased. This is contrary to the results of Schmidt and Patankar[8] who found that the transition prediction was independent of *REXMIN* for *REXMIN* less than about 1000.

From this study it can be concluded that the transition prediction is very sensitive to the grid, especially for *TU*0 =

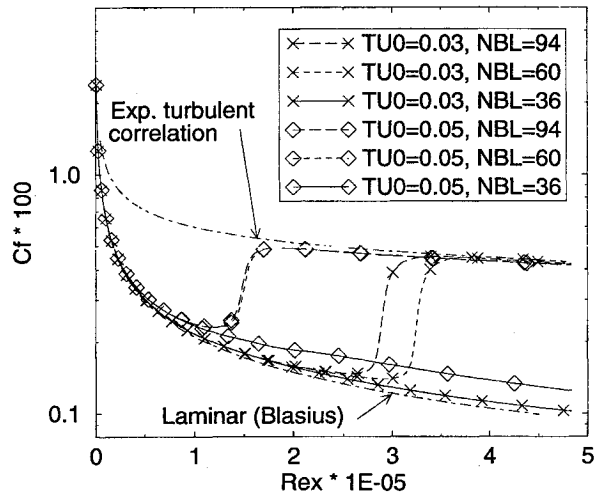

Fig. 6 Effect of near-wall grid density for transitional flat plate with BL code.

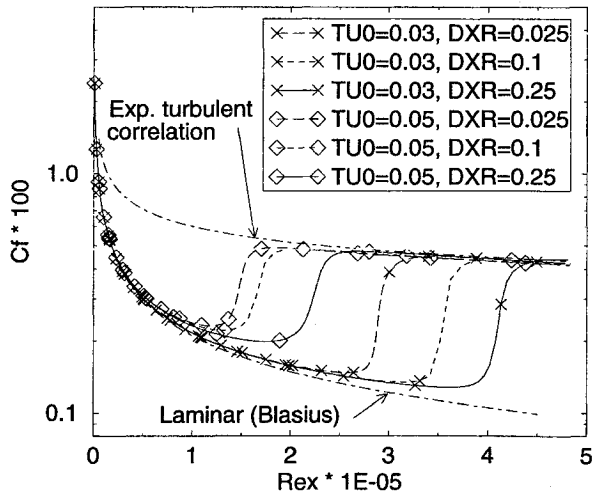

Fig. 7 Effect of streamwise grid spacing for transitional flat plate with BL code.

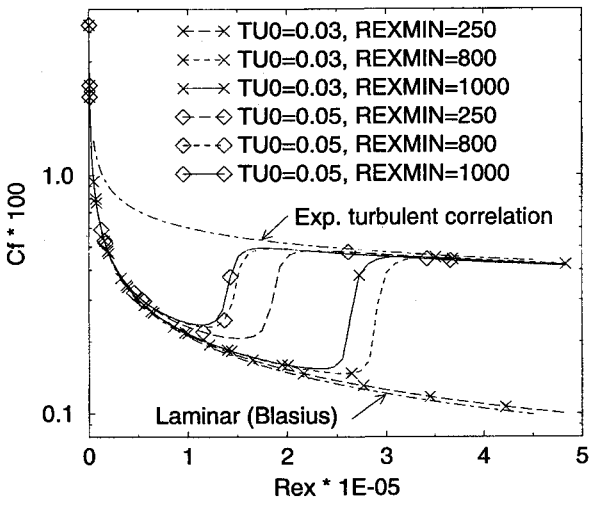

Fig. 8 Effect of starting Reynolds number for BL code.

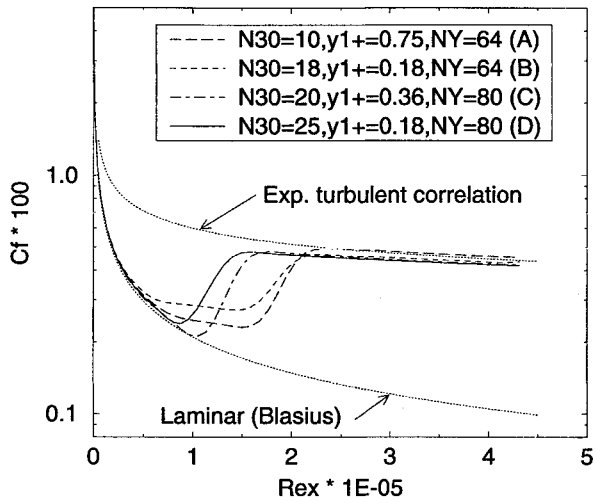

Fig. 9 Effect of near-wall grid density for transitional flat plate with NS code.

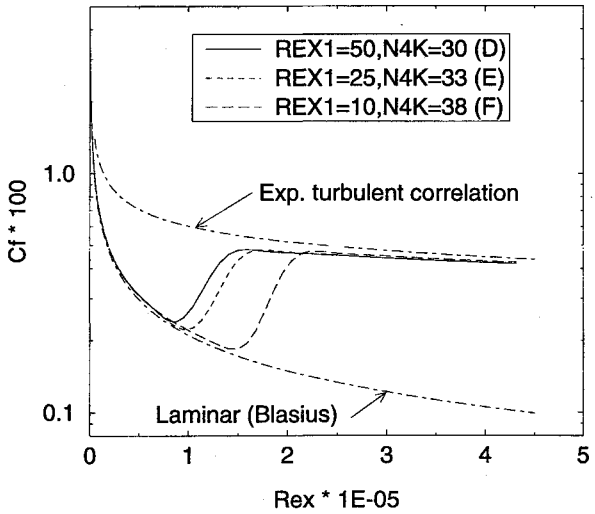

Fig. 10 Effect of streamwise grid near leading edge for transitional flat plate with NS code.

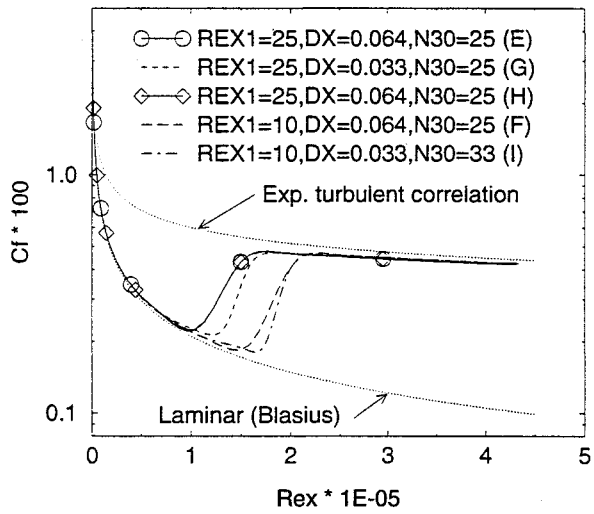

Fig. 11 Effect of grid refinement for transitional flat plate with NS code.

0.03. However, it is possible to obtain grid independent results if the near-wall and axial grid densities are sufficiently refined. The results are highly dependent on *REXMIN*, which affects the initial profiles for k and ε.

NS Code Grid Sensitivity Study

A grid study was subsequently attempted with the NS code. Grid parameters that were varied included y_1^+, *NY*, *REX*1, *NX*, and *DX*. These parameters in turn led to variations in *N*30 and *N*4*K*. As the grids were refined for this study, more problems with convergence were observed as grids with higher stretching and larger ARs were obtained. The NS code could not be run with grids as refined as those used for the BL code because of these convergence problems. However, the cases that could be converged provide valuable information about the sensitivity of the NS code predictions.

Figure 9 shows the effect of refining the near-wall grid for a fixed streamwise grid (*REX*1 = 50, *DX* = 0.064 cm, and *N*4*K* = 30). The skin friction distribution departs from the laminar distribution prematurely for low values of *N*30. As with the BL code, the NS code suggests that *N*30 must be greater than 25 to adequately resolve the k-ε profiles for transitional flow predictions.

Figure 10 shows the effect of varying the streamwise grid near the leading edge for a fixed cross-stream grid (y_1^+ = 0.18, *N*30 = 25, *NX* = 80). Investigation of the k-ε profiles for these cases revealed that as *REX*1 is decreased, the value of ε at the wall increases, leading to delayed transition.[19] Another case (case *H* in Fig. 11) was run with *N*4*K* increased from 33 to 45 by increasing *NX* from 80 to 112 with *REX*1 fixed at 25. There was no discernable difference in the transition prediction between cases *E* and *H*, indicating that the dependence was on *REX*1, not just the grid density or stretching. This is similar to the behavior observed with the BL code as *REXMIN* was decreased.

The grid spacing for the latter 75% of the grid in the streamwise direction, for which the grid spacing is uniform, was decreased from *DX* = 0.064 cm (case *E*) to *DX* = 0.033 cm (case *G*) for *REX*1 = 25. This resulted in a slight change in the transition prediction, as shown in Fig. 11. A grid with *DX* = 0.064 cm and *N*30 = 25 (case *F*) was refined both normal to the plate and in the streamwise direction to give *DX* = 0.033 cm and *N*30 = 33 (case *I*), with *REX*1 fixed at 10. The results in Fig. 11 show a relatively small change in the predicted transition location considering the general sensitivity of the predictions. Aside from the dependence on *REX*1, these grid parameters yielded acceptably small variations in the results. A set of grid parameters that offered a compromise between accuracy and convergence time were selected for further studies (y_1^+ = 0.18, *N*30 = 25, *DX* = 0.064 cm, *REX*1 = 25).

Effect of Turbulence Parameters

The ability of the LRN model to predict the transition location trends vs $TU0$ and L were investigated. Figure 12 shows the predicted skin friction for various values of $TU0$. As expected, the transition location moved upstream as $TU0$ was increased. Figure 13 shows the predicted skin friction for $TU0 = 0.03$ with various values of L. As the length scale is increased, the turbulent dissipation rate is decreased, which promotes earlier transition, as predicted. The impact on the predicted loss was determined by calculating the drag coefficient. The results from the BL code and NS code are shown in Fig. 14. Both the turbulence intensity and length scale have a marked effect on the predicted loss.

Baldwin–Lomax Model

The point transition approach with the Baldwin–Lomax algebraic turbulence model was studied with the NS code. The point transition approach involves specifying the point of transition based on experimental data or correlations. The flow is assumed laminar before this point, and the turbulent viscosity is set to zero. Aft of this point, the turbulent viscosity as determined from the turbulence model is applied. This approach is much simpler than employing a LRN k-ε model, but relies on experimental data and correlations that may not be available for complex flow conditions. For the current work, the location of the start of transition was determined from the experimental correlation given by Mayle.[1]

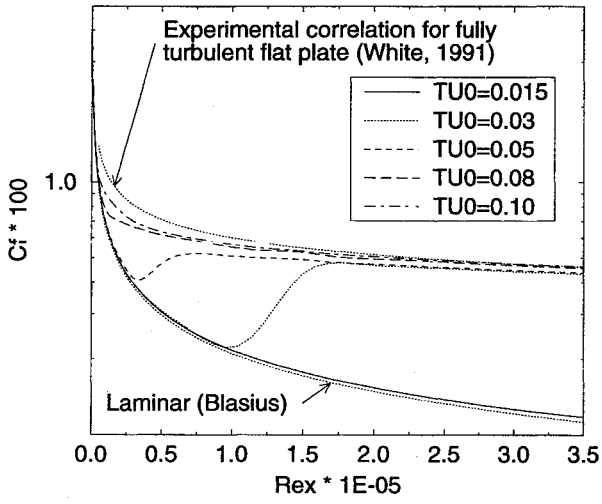

Fig. 12 Effect of inlet freestream turbulence intensity on transition prediction for NS code.

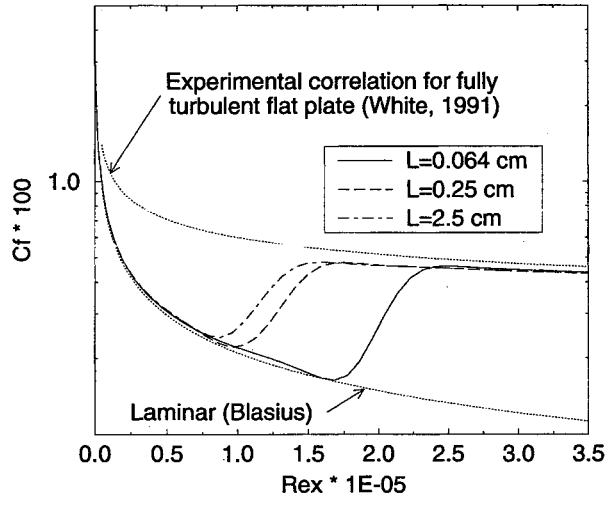

Fig. 13 Effect of inlet turbulence length scale on transition prediction for NS code.

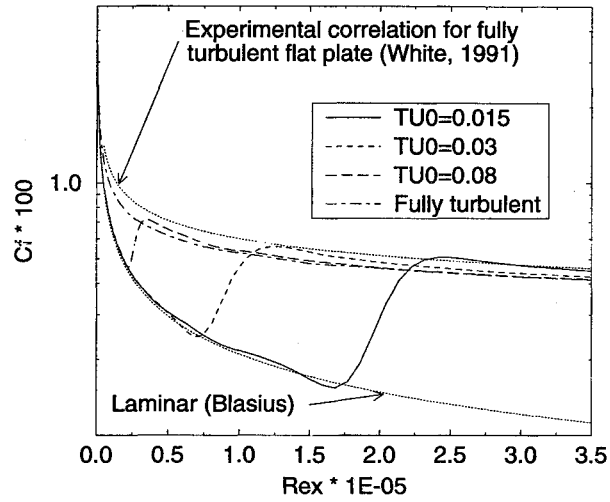

Fig. 14 Effect of inlet freestream turbulence intensity and length scale on predicted loss.

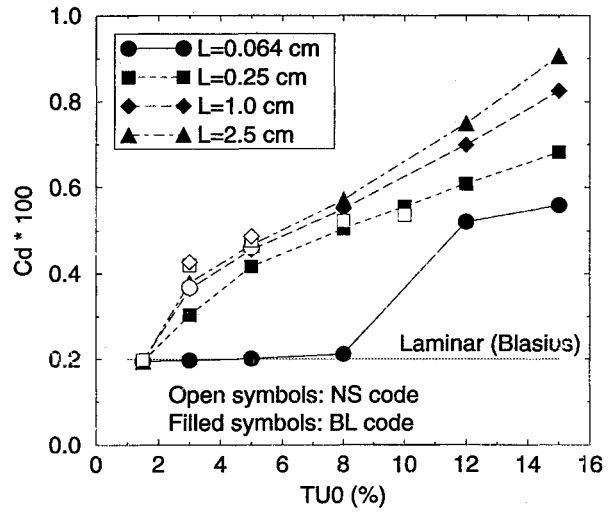

Fig. 15 Baldwin–Lomax model without wall functions ($y\dagger = 0.39$) using Mayle[1] correlation for transition location.

Figure 15 shows the predicted skin friction using this approach on a fine grid ($y_1^+ = 0.39$) without wall functions for several turbulence intensities, showing encouraging results. The same methodology was applied on a coarser grid ($y_1^+ = 50$) with wall functions for $TU0 = 0.03$, shown in Fig. 16. The resulting skin friction distribution is unacceptable, indicating that a point transition model or intermittency model cannot be used with wall functions because there is insufficient grid to resolve the laminar boundary layer upstream of transition. It also points to the need for a laminar wall function.

The ability of the NS code to predict the boundary-layer loss was assessed by calculating the drag coefficient for predictions with several different turbulence models, shown vs turbulence intensity in Fig. 17. Predictions using the BL code are also shown for comparison. Although these plots do not provide details of the transition process, transition is expected to occur in this length and they describe well the limits of the laminar and turbulent cases. As expected, the HRN k-ε model grossly overpredicts the loss for turbulence intensities below 5% compared to the other models that can account for the boundary-layer transition. The addition of a transition model in the NS code has greatly improved the loss prediction capability.

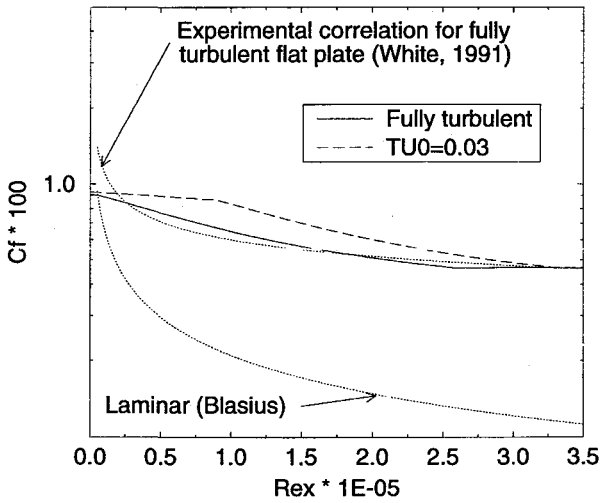

Fig. 16 Baldwin–Lomax model with wall functions ($y\dagger = 50$) using Mayle's correlation (Ref. 1) for transition location.

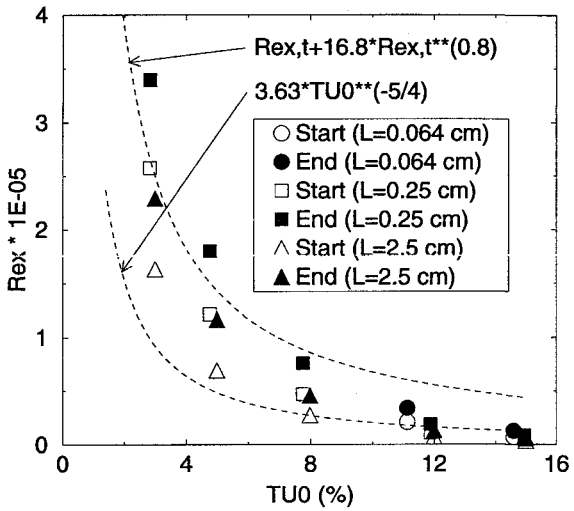

Fig. 18 Comparison of BL code results to experimental correlations for start and end of transition.

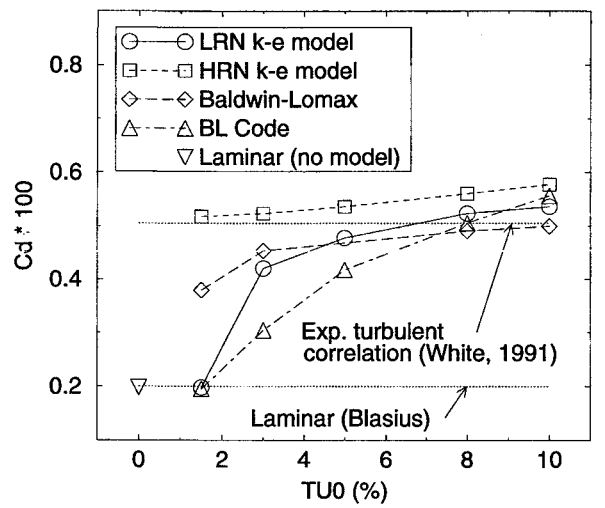

Fig. 17 Ability of NS and BL codes to predict loss.

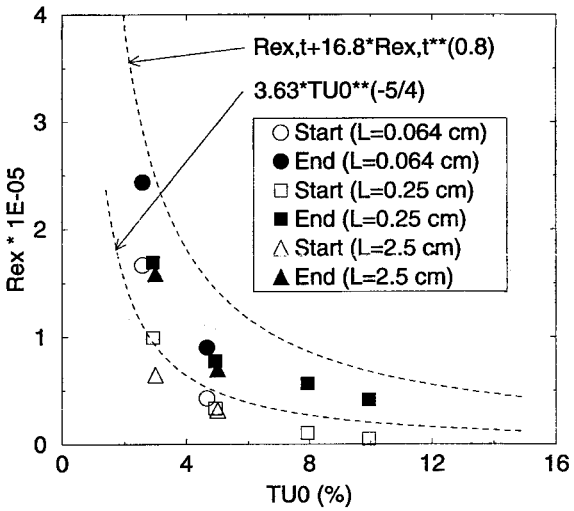

Fig. 19 Comparison of NS code results to experimental correlations for start and end of transition.

Comparison to Experimental Data

The results were compared to experimental correlations to gain further understanding about the capabilities of the model to simulate transitional flow. The correlation for the start of transition is from Mayle,[1] and the correlation for the end of transition is given by Abu-Ghannam and Shaw.[20]

Figure 18 shows the start and end of transition for the BL code predictions, and Fig. 19 shows corresponding results for the NS code. The experimental correlations are independent of length scale because the effect of length scale has not been adequately studied experimentally.[1] However, the calculations are clearly dependent on the length scale. In fact, the BL code did not predict transition for $L = 0.064$ cm for turbulence intensities below 10%. Except for high-turbulence intensities, the BL code typically predicts transition that occurs too late compared to the correlation. Figure 19, conversely, shows that the NS code typically predicts transition that occurs too early. Both codes predict transition lengths that are as much as 50% too short, with the BL code being worse.

Figures 18 and 19 also reveal that the NS code always predicts transition earlier than the BL code. The disagreement between the predicted transition locations for the two codes is attributable to differences in the numerics and assumed physics, computational grids, and initial or inlet conditions.

Modifications to the LRN model, such as those proposed by Schmidt and Patankar,[21] could be incorporated to improve the predictions of the NS code. However, the modifications they present rely on boundary-layer parameters that are difficult to define for a general, complex three-dimensional flowfield. Choi and Knight[22] have proposed alternate formulations of Schmidt and Patankar's work that do not rely on such parameters, but they did not test the proposed formulations. Developing such modifications was beyond the scope of the current work. Improved LRN k-ε models that have been developed to better predict transition, such as the one proposed by Biswas and Fukuyama,[23] should also be considered.

Conclusions

The Lam–Bremhorst LRN k-ε turbulence model has been implemented in a full three-dimensional NS flow solver in an attempt to improve the loss prediction capability for turbomachinery blade rows containing significant regions of laminar and transitional flow. The LRN model has been tested extensively with fully laminar, fully turbulent, and transitional zero pressure gradient flat plate flow at various freestream turbulence intensities and length scales. The results were compared to experimental data and a two-dimensional BL code that uses the same LRN model.

The results indicate that the NS code predicts fully laminar and fully turbulent flow well and the addition of the LRN model has improved the loss prediction for transitional flows. The chosen length scale was shown to have a large effect on the predicted loss.

The BL and NS code were both found to be sensitive to the near-wall grid and the grid near the leading edge for transitional calculations, but the grids could be sufficiently refined to obtain grid independent results. However, convergence problems associated with an explicit flow solver limited the amount of grid refinement that could be practically used. Compared to experimental data, the NS code usually predicted transition too early, while the BL code usually predicted transition too late. Both codes predicted transition lengths that were too short.

The sensitivity of the LRN model to the near-wall grid and length scale, convergence and stability problems, and excessive run times make the LRN k-ε model in an explicit NS code currently impractical for design applications. A more practical approach is the use of a point transition model with the algebraic Baldwin–Lomax model. However, this raises questions about the availability of suitable correlations for the start of transition for complex flows such as in turbomachinery blade rows.

Acknowledgments

The first author would like to thank Mark G. Turner, Senior Staff Engineer at General Electric Aircraft Engines, for the many helpful discussions during the course of this work. The authors wish to acknowledge General Electric Aircraft Engines for permission to publish this article.

References

[1]Mayle, R. E., "The Role of Laminar-Turbulent Transition in Gas Turbine Engines," American Society of Mechanical Engineers Paper 91-GT-261, June 1991.

[2]Cumpsty, N. A., *Compressor Aerodynamics*, Longman Scientific and Technical, New York, 1989.

[3]Turner, M. G., and Jennions, I. K., "An Investigation of Turbulence Modeling in Transonic Fans Including a Novel Implementation of an Implicit k-ε Turbulence Model," *Journal of Turbomachinery*, Vol. 115, No. 2, 1993, pp. 249–260.

[4]Jennions, I. K., and Turner, M. G., "Three-Dimensional Navier-Stokes Computations of Transonic Fan Flow Using an Explicit Flow Solver and an Implicit k-ε Solver," *Journal of Turbomachinery*, Vol. 115, No. 2, 1993, pp. 261–272.

[5]Turner, M. G., Liang, T., Beauchamp, P. P., and Jennions, I. K., "The Use of Orthogonal Grids in Turbine CFD Computations," American Society of Mechanical Engineers Paper 93-GT-38, May 1993.

[6]Baldwin, B. S., and Lomax, H., "Thin Layer Approximation and Algebraic Model for Separated Turbulent Flows," AIAA Paper 78-257, Jan. 1978.

[7]Launder, B. E., and Spalding, D. B., "The Numerical Computation of Turbulent Flows," *Computer Methods in Applied Mechanics and Engineering*, Vol. 3, No. 2, 1974, pp. 269–289.

[8]Schmidt, R. C., and Patankar, S. V., "Simulating Boundary Layer Transition with Low-Reynolds-Number k-ε Turbulence Models: Part 1—An Evaluation of Prediction Characteristics," *Journal of Turbomachinery*, Vol. 113, No. 1, 1991, pp. 10–17.

[9]Lam, C. K. S., and Bremhorst, K., "A Modified Form of the k-ε Model for Predicting Wall Turbulence," *Journal of Fluids Engineering*, Vol. 103, No. 3, 1981, pp. 456–460.

[10]Rodi, W., and Scheuerer, G., "Calculation of Heat Transfer to Convection-Cooled Gas Turbine Blades," *Journal of Engineering for Gas Turbines and Power*, Vol. 107, No. 3, 1985, pp. 620–627.

[11]Fujisawa, N., "Calculations of Transitional Boundary Layers with a Refined Low Reynolds Number Version of a k-ε Model of Turbulence," *Proceedings of the International Symposium on Engineering Turbulence Modelling and Measurements*, Dubrovnik, Yugoslavia, Sept. 1990, pp. 23–32.

[12]Stephens, C. A., and Crawford, M. E., "An Investigation into the Numerical Prediction of Boundary Layer Transition Using the K.Y. Chien Turbulence Model," NASA-CR-185252, June 1990.

[13]Martinelli, L., "Calculations of Viscous Flows with a Multigrid Method," Ph.D. Dissertation, Princeton Univ., Princeton, NJ, 1987.

[14]Zerkle, R. D., and Lounsbury, R. J., "Freestream Turbulence Effect on Turbine Airfoil Heat Transfer," *Journal of Propulsion*, Vol. 5, No. 1, 1989, pp. 82–88.

[15]Patankar, S. V., and Spalding, D. B., *Heat and Mass Transfer in Boundary Layers*, 2nd ed., International Textbook, London, 1970.

[16]Patel, V. C., Rodi, W., and Scheuerer, G., "Turbulence Models for Near-Wall and Low Reynolds Number Flows: A Review," *AIAA Journal*, Vol. 23, No. 9, 1985, pp. 1308–1319.

[17]Kunz, R. F., and Lakshminarayana, B., "Explicit Navier-Stokes Computation of Cascade Flows Using the k-ε Turbulence Model," *AIAA Journal*, Vol. 30, No. 1, 1992, pp. 13–22.

[18]White, F. M., *Viscous Fluid Flow*, McGraw–Hill, New York, 1991.

[19]Dailey, L. D., "Simulating Laminar-Turbulent Transition with a Low Reynolds Number k-ε Turbulence Model in a Navier-Stokes Flow Solver," M.S. Thesis, Univ. of Cincinnati, Cincinnati, OH, 1993.

[20]Abu-Ghannam, B. J., and Shaw, R., "Natural Transition of Boundary Layers—The Effects of Turbulence, Pressure Gradient, and Flow History," *Journal of Mechanical Engineering Science*, Vol. 22, No. 5, 1980, pp. 213–228.

[21]Schmidt, R. C., and Patankar, S. V., "Simulating Boundary Layer Transition with Low-Reynolds-Number k-ε Turbulence Models: Part 2—An Approach to Improving the Predictions," *Journal of Turbomachinery*, Vol. 113, No. 1, 1991, pp. 18–26.

[22]Choi, D., and Knight, C. J., "Improved Turbulence Modeling for Gas Turbine Application," AIAA Paper 91-2239, June 1991.

[23]Biswas, D., and Fukuyama, Y., "Calculation of Transitional Boundary Layers with an Improved Low-Reynolds Number Version of the k-ε Turbulence Model," American Society of Mechanical Engineers Paper 93-GT-73, May 1993.